

General theory of the transverse dielectric constant of III-V semiconducting compounds

K. B. Kahen and J. P. Leburton

Department of Electrical Engineering and Coordinated Science Laboratory, University of Illinois at Urbana-Champaign, Urbana, Illinois 61801

(Received 22 April 1985; revised manuscript received 24 June 1985)

We have developed a general model of the transverse dielectric constant of III-V compounds using a hybrid method which combines the $\mathbf{k}\cdot\mathbf{p}$ method with a nonlocal pseudopotential calculation. In our method we partition the Brillouin zone into three regions by expanding the energy bands and matrix elements about the Γ , X , and L symmetry points. The real and imaginary parts of the dielectric constant are calculated as a sum of the individual contributions of each region. By using this partition method, we are able to get good insight into the dependence of the dielectric constant on the shape of the band structure. Hence, it is seen that the X and L regions contribute 90–95% and the Γ region only 5–10% to the zero-frequency dielectric constant. In general, our results for $\epsilon_1(0)$ and $\epsilon_2(\omega)$ agree well with the experimental data.

I. INTRODUCTION

In the past two decades there has been considerable experimental^{1–5} and theoretical^{6–10} interest in the determination of the optical properties of III-V semiconducting compounds. From a general standpoint, all of the optical properties of materials can be evaluated through a calculation of the complex dielectric constant, $\epsilon(\omega) = \epsilon_1(\omega) + i\epsilon_2(\omega)$. As this calculation requires the knowledge of the entire band structure of a material, it is necessary to determine the wave functions and energy bands throughout the irreducible region of the first Brillouin zone. A number of band-structure techniques, for example, orthogonal plane wave^{6,7} (OPW), augmented plane wave⁸ (APW), pseudopotential,⁹ and linear combination of Gaussian orbitals¹⁰ (LCGO), have been implemented to calculate, with varying success, the dielectric constant of bulk semiconductors. However, these different theoretical approaches employ sophisticated computational methods which require extended running times. Hence, with most of these models it is difficult to assess the relative importance of band-structure parameters such as effective masses and optical matrix elements in determining the value of the real part of the transverse dielectric constant. Also, the relative contributions to $\epsilon_1(\omega)$ of the different regions of the Brillouin zone, Γ , X , and L , are not easily discernible. These problems become acute when inhomogeneity, interfaces, or spatial variation of the chemical composition x of the material, for example, $\text{Al}_x\text{Ga}_{1-x}\text{As}$ with x varying with distance, modify the translational invariance of bulk semiconductors and alter their electronic and optical properties without affecting drastically the host crystal structure. Man-made superlattices^{11,12} are an example of these structures which have a high potential for applications in optoelectronics,¹³ and which are presently under intensive investigation. Previously,¹⁴ we have calculated the index of refraction of AlAs-GaAs superlattices by using the partition method mentioned above. It is the purpose of this paper to introduce formally the method, presenting some results for

bulk III-V compounds and discussing the merits of the technique.

Our approach is based on the $\mathbf{k}\cdot\mathbf{p}$ method.¹⁵ In this technique the band structure is generated by expanding the energies and wave functions about one or several symmetry points. As will be discussed in this paper, the majority of low-energy optical transitions, $\hbar\omega < 6$ eV, originate from regions near the main symmetry points Γ , X , and L . Furthermore, because they are the highest symmetry points, it is mathematically straightforward to obtain expansions about these points, leading to a partition of the Brillouin zone. The $\mathbf{k}\cdot\mathbf{p}$ band parameters are fitted empirically with experimental energy gaps and effective masses, when available; otherwise, these parameters are estimated from nonlocal pseudopotential calculations which include spin-orbit effects. Since the band parameters are fitted using experimental data, the $\mathbf{k}\cdot\mathbf{p}$ method reproduces very accurately the band structure in the vicinity of the expansion points. Therefore, our approach appears as a hybrid model, combining the advantages of the $\mathbf{k}\cdot\mathbf{p}$ method with the generality of the pseudopotential method. The dielectric constant is then calculated as the sum of the contributions of these different Brillouin-zone regions. Because our method considers each region separately, it engenders a physical understanding of the parameters which affect the dielectric constant. Moreover, it is sufficiently flexible to include secondary effects, for example, excitons and band tailing, and it is computationally fast.

The paper is organized in the following manner. In Sec. II we discuss the formation of the $\mathbf{k}\cdot\mathbf{p}$ band structure for III-V compounds and present a table of the band-edge valence and conduction-band effective masses at the Γ , X , and L points for each of five III-V compounds, GaP, GaAs, InP, InAs, and AlAs. To our knowledge, this is the first time that effective masses at Γ , X , and L have been given for all five III-V compounds. In Sec. III we present the formulation of the complex dielectric constant and describe the partition method used to perform the computations. In Sec. IV we discuss our results for the

five III-V compounds, comparing the real and imaginary parts of the dielectric constant with the experimental data. Special emphasis is given to the determination of $\epsilon_1(0)$ in terms of the contributions of the Γ , X , and L regions because it is directly related to the index of refraction of the materials, and, to our knowledge also, it is the first time they have been reported.

II. $\mathbf{k}\cdot\mathbf{p}$ METHOD AND BRILLOUIN-ZONE PARTITION

In this section the discussion of the $\mathbf{k}\cdot\mathbf{p}$ method will be limited to points where our implementation differs from the standard technique. The reader is referred to papers by Kane^{15,16} and Dresselhaus¹⁷ for general theory and applications to III-V compounds. Using the $\mathbf{k}\cdot\mathbf{p}$ method, the entire structure can be obtained by expanding about one symmetry point; however, this requires a large basis set and matrix Hamiltonian. Since one of our goals is to be able to predict and understand the optical properties of III-V compounds in general, it is desirable to have simple, analytical expressions for the energy bands and matrix elements. Consequently, we expand about three symmetry points, Γ , X , and L , and use a small number of bands in each of our $\mathbf{k}\cdot\mathbf{p}$ basis sets, therefore, limiting the accuracy of the energy-band expressions to regions surrounding the expansion points. Because of the size of the X and L regions, it is necessary to supplement the X - and L -point expansions by ones about the K and W points also. However, because of the low symmetry characterizing these points, it is difficult to obtain the energy dispersion relations and optical matrix elements in the volumes surrounding these two points. Therefore, for both the K and W points, the energy expressions and matrix elements are obtained directly from the pseudopotential calculations.

In order to evaluate the dielectric constant for energies less than 6 eV, it is reasonable to restrict the calculation to transitions between band-edge states where the transition rates are the largest. Consequently, in performing the energy expansions about Γ , X , and L we treat the band-edge states exactly and incorporate the effects of the other bands (Löwdin states) using a perturbation technique described by Löwdin.^{16,18} The renormalizations are performed by including only those bands which give the largest contributions. This approximation results in a slight overestimation of the matrix elements involving these bands. This point will be discussed in more detail later in the paper. In all of our Löwdin states, we find it necessary to add d -symmetry states onto those states of Γ_{15} symmetry in order to obtain the correct energy-band curvatures. This idea was suggested by Chadi,^{19,20} who showed from pseudopotential calculations that there is appreciable mixing of d -symmetry states onto the Γ_{15} states, and in a type of tight-binding calculation, he determined that the addition of d -symmetry states to a s - p basis set results in more accurate wave functions and energy bands.

Our energy expansion about Γ is a simplification of the one given by Kane.¹⁶ We assume the energy is isotropic

and only consider renormalization involving the lowest Γ_{15} conduction states. The neglect of the Γ_1 valence state and the lowest Γ_{12} conduction states is reasonable because of the strength of the s - p wave-function interaction. The X - and L -point expansions have only been discussed briefly by both Kane¹⁶ and Dresselhaus,¹⁷ consequently, in Sec. II A we give the basis sets and renormalized matrices for both regions.

A. X -point region

The eight X -point basis states are

$$\begin{aligned} X_5 & \begin{cases} iz\uparrow, \\ y\uparrow, \end{cases} \\ X_1^c & s^c\uparrow, \end{aligned} \quad (1a)$$

$$X_5^c \frac{1}{\sqrt{2}}(ix^c + id_{yz}^c)\uparrow,$$

$$X_1 \frac{1}{\sqrt{2}}(s + f_{xyz})\uparrow,$$

$$X_3 \frac{1}{\sqrt{2}}(ix + id_{yz})\uparrow, \quad (1b)$$

$$X_5^c \begin{cases} iz^c\uparrow, \\ y^c\uparrow. \end{cases}$$

In the above we have labeled the wave functions using single-group symmetry notation. The superscript c signifies a conduction-band state (no superscript in the above implies a valence-band state); x , y , and z are the three orthogonal components of the p -symmetry state; and d_{yz} and f_{xyz} are d - and f -symmetry states transforming as yz and xyz , respectively. The states listed in (1a) are treated exactly while those in (1b) are incorporated by Löwdin renormalization. In Eqs. (1) we choose the $\langle 100 \rangle$ axis to lie along the x direction. The X_1 wave function has an f -symmetry state for reasons analogous to those discussed previously for the d -symmetry states.^{19,20} The same band structure results from the above basis set with spin down. Because the energy gaps at the X point for III-V semiconductors are large, we find it reasonable to diagonalize two 2×2 matrices instead of one 4×4 matrix. The resulting 2×2 matrices are

$$\begin{pmatrix} k_z^2[(E1) + \frac{1}{2}(E2)] + \frac{\hbar^2 k^2}{2m_0} & \frac{1}{2}\Delta' \\ \frac{1}{2}\Delta' & \frac{1}{2}k_z^2(H' + I) + \frac{\hbar^2 k^2}{2m_0} \end{pmatrix}, \quad (2a)$$

$$\left[\begin{array}{c} E_{3,x}^c + \frac{1}{4} D k_x^2 + \frac{1}{2} k_z^2 (-H' + G) + \frac{\hbar^2 k^2}{2m_0} \\ k_x \left[\frac{F(E_{1,x}^c - E_{5,x}^c)}{2} \right]^{1/2} \\ E_{1,x}^c + \frac{(E1)(E_{5,x} - E_{1,x}^c) k_x^2}{2(E_{1,x}^c - E_{3,x})} + k_z^2 [F - (E1)] + \frac{\hbar^2 (k_x'^2 + k_z^2)}{2m_0} \end{array} \right] k_x \left[\frac{F(E_{1,x}^c - E_{5,x}^c)}{2} \right]^{1/2} \quad (2b)$$

Equations (2a) and (2b) are for the band-edge valence and conduction bands, respectively. In Eqs. (2) we choose the z direction as the arbitrary (neglecting the anisotropy) perpendicular direction and the top of the valence band as the zero of energy. k_x and k_z are the k vectors along the $\langle 100 \rangle$ and z directions, respectively, and $k_x' = k_x - k_m$, where k_m corrects for the X_1^c minimum not being at the X point. k_m is determined empirically from the pseudopotential calculations. Δ' is the spin-orbit constant defined analogously to Kane's¹⁶ Δ , and $E_{1,x}^c$, for example, is the relative energy of the X_1^c state. D , $(E1)$, $(E2)$, F , G , H' , and I are the Löwdin coefficients and are defined similarly to L , M , and N of Dresselhaus *et al.*²¹ The parameters in Eqs. (2) are fitted empirically by computer so that the X_1 , X_3 , X_5 , X_1^c , and X_3^c bands all have the correct relative position and dispersion relations.

B. L region

The ten L -point basis states are

$$\begin{aligned} L_3 & \frac{i}{\sqrt{2}}(x-y)\uparrow, \\ L_3 & \frac{1}{\sqrt{6}}(2z-x-y)\uparrow, \\ L_1^c & s^c\uparrow, \end{aligned} \quad (3a)$$

$$\begin{aligned} L_1 & \frac{1}{\sqrt{2}}(s + f_{xyz})\uparrow, \\ L_1 & \frac{i}{\sqrt{6}}(x+y+z+d_{xy}+d_{xz}+d_{yz})\uparrow, \\ L_3^c & \left[\begin{array}{l} \frac{i}{\sqrt{2}}(x^c - y^c + d_{yz}^c - d_{xz}^c)\uparrow, \\ \frac{1}{\sqrt{12}}(2z^c - x^c - y^c + 2d_{xy}^c - d_{yz}^c - d_{xz}^c)\uparrow, \end{array} \right] \\ L_2^c & \frac{i}{\sqrt{6}}(x^c + y^c + z^c + d_{xy}^c + d_{xz}^c + d_{yz}^c)\uparrow, \\ L_3^c & \left[\begin{array}{l} \frac{1}{\sqrt{6}}(2d_{z^2}^c - d_{x^2}^c - d_{y^2}^c)\uparrow, \\ \frac{i}{\sqrt{2}}(d_{x^2}^c - d_{y^2}^c)\uparrow. \end{array} \right] \end{aligned} \quad (3b)$$

The states listed in (3a) are treated exactly and those in (3b) are incorporated using Löwdin renormalization. For convenience, we take the spin quantization axis to be the $\langle 111 \rangle$ axis. Using this coordinate system for the spin-orbit interaction, H_{SO} only connects L_3 states having the same spin. The basis set with spin down is degenerate with the states listed in Eqs. (3).

Similar to the X -region treatment, because of the large band gap at the L point, we diagonalize a 2×2 matrix consisting of the two upper valence bands and consider separately the lowest conduction band. The 2×2 matrix is written as

$$\left[\begin{array}{c} \frac{1}{2m_0} \hbar^2 k^2 + \frac{1}{6} T k_l^2 + \frac{1}{3} k_t^2 (T + \frac{1}{2} V') \\ \frac{1}{2} \Delta'' \\ \frac{1}{2} \Delta'' \\ \frac{1}{2m_0} \hbar^2 k^2 + \frac{1}{6} T k_l^2 + k_t^2 \left[\frac{1}{3} T + \frac{1}{2} U + \frac{1}{6} (V' + W) - \frac{S(E_{1,L}^c - E_{1,L})}{E_{1,L}^c - E_{3,L}} \right] \end{array} \right] \frac{1}{2} \Delta'' \quad (4a)$$

and the dispersion relation for the L_1^c band is

$$E = E_{1,L}^c + \frac{1}{2m_0} \hbar^2 k^2 + \frac{1}{2} k_l^2 (R + S) + k_t^2 \left[\frac{S(E_{1,L}^c - E_{1,L})}{E_{1,L}^c - E_{3,L}} + \frac{R(E_{1,L}^c - E_{2,L}^c)}{2(E_{1,L}^c - E_{3,L})} \right]. \quad (4b)$$

In Eqs. (4), k_l and k_t are the longitudinal and transverse k basis vectors, respectively. k_l is taken along the L - Γ direction and k_t is arbitrarily, by symmetry, taken along the L - W direction. In analogy with the X -region treatment, Δ'' is the spin-orbit constant; $E_{1,L}^c$ is the relative

energy of the L_1^c state, for example; and R , S , T , U , V' , and W are the Löwdin coefficients. Again, the parameters are fitted empirically so that the L_1 , L_1 , L_3 , and L_1^c bands have the correct relative positions and dispersion relations.

TABLE I. Low-temperature theoretical and experimental band-edge masses at the Γ , X , and L symmetry points. Each of the experimental masses is referenced. For Γ only the density-of-states masses are given while for X and L both the longitudinal and transverse masses are presented.

	GaAs	AlAs	InAs	InP	GaP
$\Gamma_1^c m^*$	0.067 ^a	0.140	0.023 ^{b,c}	0.077 ^b	0.122
$\Gamma_{hh}^v m^*$	-0.510 ^a	-0.536	-0.40 ^d	-0.58 ^e	-0.56 ^e
$\Gamma_{lh}^v m^*$	-0.082 ^a	-0.087	-0.026 ^d	-0.12 ^e	-0.16 ^e
$\Gamma_{so}^v m^*$	-0.154 ^a	-0.217	-0.166	-0.179	-0.289
$L_6^c m_l$	1.854	1.592	2.333	2.149	1.988
m_t	0.136	0.157	0.143	0.144	0.147
$L_{4,5}^v m_l$	1.731	2.011	1.668	2.021	1.948
m_t	-0.277	-0.290	-0.308	-0.295	-0.278
$L_6^v m_l$	1.731	2.011	1.668	2.021	1.948
m_t	-0.277	-0.290	-0.308	-0.295	-0.278
$X_7^c m_l$	0.495	0.385	0.593	0.566	0.551
m_t	0.258	0.254	0.305	0.279	0.249
$X_6^c m_l$	2.100	1.158	4.516	2.772	1.70 ^f
m_t	0.277	0.268	0.307	0.278	0.191 ^f
$X_7^v m_l$	1.209	1.300	1.236	1.341	1.258
m_t	-0.744	-0.659	-1.109	-0.839	-0.628
$X_6^v m_l$	1.209	1.300	1.236	1.341	1.258
m_t	-0.744	-0.659	-1.109	-0.839	-0.628

^aReference 22.

^bReference 23.

^cReference 24.

^dReference 25.

^eReference 26.

^fReference 27.

C. Effective masses

Table I lists the low-temperature (5–77 K) values of the band-edge effective masses at the three symmetry points for the five III-V compounds. Presented are the longitudinal and transverse masses for the X and L states and the density-of-states masses for the Γ states. When experimental data is not available, the masses are calculated using the results of nonlocal pseudopotential calculations which include the spin-orbit interaction. These masses along with the energy gaps are used to determine the direct interaction and Löwdin coefficients at the three symmetry points. Instead of taking the masses directly from the energy-band curvatures, a technique with a fair amount of uncertainty, the mass m^* at the point \mathbf{k}_0 is calculated using¹⁶

$$\frac{1}{m^*} = \frac{1}{m_0} + \frac{2\hbar^2}{m_0^2} \sum_{n'} \frac{|\mathbf{s} \cdot \nabla_{nn'}|^2}{E_n(\mathbf{k}_0) - E_{n'}(\mathbf{k}_0)}, \quad (5)$$

where \mathbf{s} is a unit vector in the direction of a principal axis, $\nabla_{nn'}$ is the gradient operator between the states n and n' at the point \mathbf{k}_0 , and the summation is over all $n' \neq n$.

In order to test the accuracy of our masses, we calculated the conduction-band masses at Γ for GaAs, InP, and InAs for which experimental data are available. The masses are 0.070, 0.075, and 0.028 for GaAs, InP, and InAs, respectively. As can be seen, our calculated masses compare favorably with the experimental data.

III. DIELECTRIC-CONSTANT FORMULATION

The dielectric constant is calculated as the sum of interband optical transitions. As stated previously, we only consider transitions between the highest valence-band states and the lowest conduction-band states. Consequently, for the Γ -region contribution we include transitions between the upper three valence bands and the lowest conduction band, for the X -region contribution we include transitions between the upper two valence bands and the two lowest conduction bands, and for the L -region contribution we include transitions between the upper two valence bands and the lowest conduction band. In Fig. 1, arrows on the GaAs band structure represent the aforementioned interband transitions. In our model both the L and X regions include the K and W points, even though Fig. 1 only shows the K point as being part of the X region.

Because of our restriction to band-edge transitions, we have to calculate both the real and imaginary parts of the dielectric constant since the Kramers-Kronig relation²⁸ cannot be used to determine $\epsilon_1(\omega)$ as a function of $\epsilon_2(\omega)$ since $\epsilon_2(\omega)$ is only computed for a limited range of energies. Explicit formulas for $\epsilon_1(\omega)$ and $\epsilon_2(\omega)$ are given by Bassani and Parravicini.²⁸ In evaluating $\epsilon(\omega)$, we ignore excitonic effects and assume the valence band is filled and the conduction band is empty.

In calculating the dielectric constant, the summation

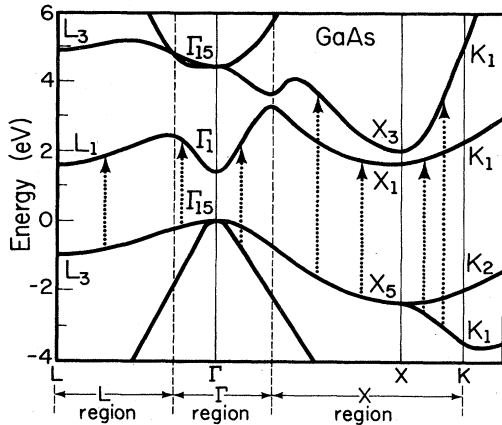


FIG. 1. Optical transitions between the band-edge valence and conduction bands for the three regions, Γ , X , and L , for GaAs. Only these transitions are included in our model.

over \mathbf{k} states is replaced by an integration over the first Brillouin zone. Since we calculate the dielectric constant by summing over the contributions of the regions around the Γ , X , and L points, the integration is performed separately for each region. The integration volumes for the Γ , X , and L regions are approximated by a sphere and two cones, respectively (see Fig. 2). For GaAs, the volumes of these regions, taking into account the sixfold and eightfold degeneracies of the X and L regions, respectively, are 8.24×10^{-2} , 1.35, and 4.01 \AA^{-3} for Γ , X , and L , respectively. The total volume of 5.44 \AA^{-3} is less than 1% different from the actual volume of the first Brillouin zone of GaAs.

The integration over the Γ region is straightforward since we assume the region to be isotropic. The integrations over the X and L regions are performed analogously and are accomplished in the following manner. We incorporate the anisotropy of the two regions into our model by performing $\mathbf{k} \cdot \mathbf{p}$ expansions from both points towards the Γ , K , and W points. Using the results of non-local pseudopotential calculations, we also obtain analyti-

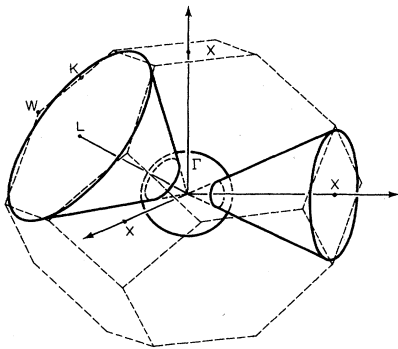


FIG. 2. Partition of the first Brillouin zone of a zinc-blende lattice into the Γ , X , and L regions. The Γ region is a sphere while the X and L regions are both cones. The K and W points are also part of the X region.

cal expressions for expansions from K and W towards the Γ , X , and L points. For simplicity, the energies and matrix elements between the expansion lines are computed by linear interpolation. By comparing these interpolated values with those resulting from a nonlocal pseudopotential calculation, we have determined that our linear interpolation approximation, in spite of its roughness, yields reasonable results. Having obtained analytical expressions for the dispersion relations, we are able to obtain the energies and matrix elements at a large number of mesh points using a small amount of computation time.

IV. RESULTS AND DISCUSSION

Figures 3 compare our calculated $\epsilon_2(\omega)$ curves with the experimental data of Aspnes and Studna.²⁹ As the theoretical curves are generated using low-temperature (5 K) band-structure data while the experimental data are obtained at 300 K, we have shifted the experimental curves by 0.1 eV in order to account for this difference. Experimental data does not exist for AlAs.

The most noticeable feature of all of the curves is the presence of the two well-known E_1 and E_2 peaks. The E_1 peak arises from transitions occurring over a large portion of the Brillouin zone around the L points. There is no E_1 peak for AlAs because the L - and K -point energy gaps differ by less than 1 eV; hence, the position of the AlAs E_1 peak overlaps with the low-energy slope of its E_2 peak. Except for InAs and GaAs for which our theoretical curves show a small structure due to the L -point spin-orbit splitting, the Ga and In compounds exhibit unsplit E_1 peaks which are broader than the experimental peaks. We believe that this occurs mainly because of the absence of excitons in our model. Exciton effects might have various consequences on the magnitudes of the E_1 peaks because they alter both the density of states and the optical matrix elements. According to Velicky and Sak³⁰ and Hanke and Sham,³¹ excitons should sharpen and enhance the E_1 peak. We account qualitatively for their results by the following argument. Without excitons, the E_1 peak arises from transitions away from the L - Γ line because the band-edge conduction and valence bands along that line have small transverse masses and, correspondingly, small densities of states which are insufficient to support a peak. Consequently, the peak is shifted to higher energies where the phase space is larger. Exciton effects should lower the L gap and raise the transverse effective masses, resulting in higher densities of states along the L - Γ line. Thus, the structure of the line would be reflected in the shape of the E_1 peak, i.e., the peak would become split.

These ideas are corroborated by our theoretical results. The InAs band-edge matrix elements are a factor of 2 smaller than those of GaP; however, InAs has the largest E_1 peak. Furthermore, its peak is the sharpest and the most centered of the four compounds. This occurs because its transverse energy-band curvature is the smallest among these compounds; hence, the E_1 peak is supported mainly by transitions occurring close to the L - Γ line. However, for more precise information, an explicit calculation is required to determine the overall effect of exci-

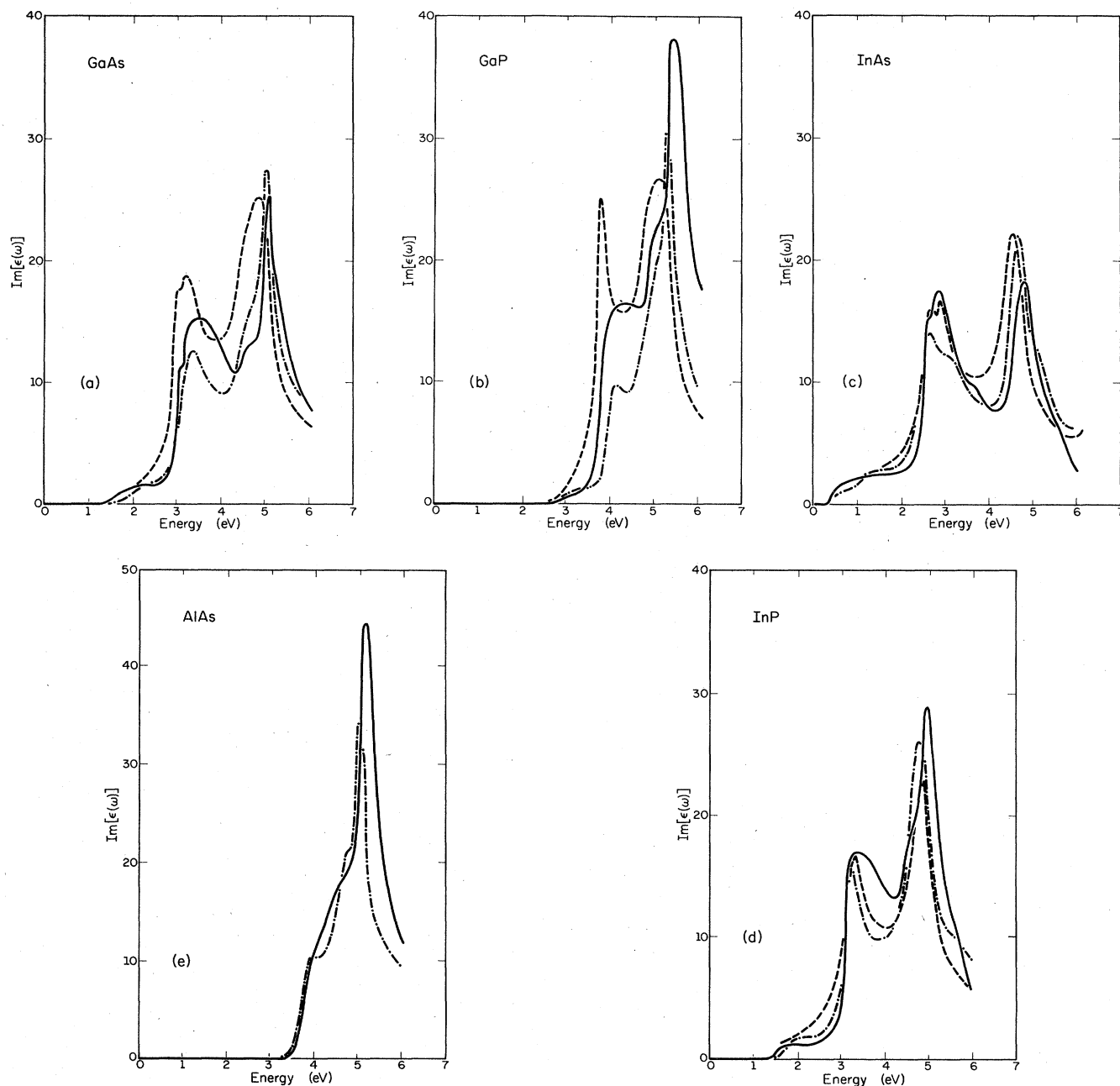


FIG. 3. Imaginary part of the dielectric constant of five III-V compounds. The solid and dot-dashed lines are calculated by the $\mathbf{k} \cdot \mathbf{p}$ and nonlocal pseudopotential methods, respectively, while the dashed line is the experimental results. (a), (b), (c), (d), and (e) are for GaAs, GaP, InAs, InP, and AlAs, respectively. The experimental data are extrapolated to 5 K.

tions on the E_1 peak. This will be treated in a forthcoming paper.³²

The E_2 peak originates from a region around the special \mathbf{k} point $(\frac{3}{4}, \frac{1}{4}, \frac{1}{4})$ as suggested by Aspnes³³ and computed by Chelikowsky and Cohen.³⁴ From our calculations, we find that the density of states in this region is more important than the magnitude of the optical matrix elements in influencing the strength of the E_2 peak. Excitons should lower the E_2 peak.^{30,31} A possible explanation

is that excitons could disrupt the parallel-band curvature in the vicinity of the special \mathbf{k} point. This would lower the effective density of states in this region and, consequently, reduce the E_2 peak. The same exciton effect can account for the slight energy difference between the experimental and theoretical curves for GaAs, GaP, InAs, and InP.

The other regions of the Brillouin zone have small contributions to the dielectric constant in the (0–6) eV range.

The Γ -valley contribution is negligible because of its small phase space as shown in Sec. III. The X -region contribution is small because its phase space and matrix elements are, respectively, about a factor of 3 and 2 smaller than those of the L region.

A. Comparison with pseudopotential

Figures 3 also compare our results with those generated using a nonlocal pseudopotential calculation. The spin-orbit interaction is not included in the pseudopotential calculations. For GaP, the effect of the omission is negligible; however, for the other four compounds, the spin-orbit interaction effectively lowers the important band gaps by ~ 0.1 eV. Consequently, for these four compounds, we have shifted the $\epsilon_2(\omega)$ curves so that the L -point energy gaps agree with the spin-orbit results. From $\mathbf{k}\cdot\mathbf{p}$ theory, it can be shown that this is a good approximation since the spin-orbit interaction only shifts the bands, having a small effect on the band curvatures and matrix elements at L , X , and K .

The results of our model compare favorably with both the experimental and pseudopotential results. The magnitudes of our E_1 peaks are larger and more closely approximate the experimental peaks than those determined by the pseudopotential calculations. For GaAs, InAs, and InP, the E_2 peaks calculated by the $\mathbf{k}\cdot\mathbf{p}$ and pseudopotential methods are comparable in magnitude, but, slightly shifted with respect to the experimental E_2 peaks, while, for AlAs and GaP, the $\mathbf{k}\cdot\mathbf{p}$ peaks are substantially larger than the pseudopotential peaks. The discrepancy in the magnitudes of the E_1 and E_2 peaks calculated by the $\mathbf{k}\cdot\mathbf{p}$ and pseudopotential methods can be attributed to the difference in the values of the optical matrix elements and to our linear interpolation approximation of the off-expansion line energies as discussed in Sec. III. As stated previously, the $\mathbf{k}\cdot\mathbf{p}$ matrix elements involving the Löwdin states are overestimated due to the neglect of all but the closest higher bands of the proper symmetry.³⁵ However, we found that the band-edge $\mathbf{k}\cdot\mathbf{p}$ and pseudopotential matrix elements differ by only a few percent. This result agrees with the calculation of Hermann and Weisbuch³⁵ who found that the Γ -point band-edge matrix elements are insensitive to the higher-band contributions. Since the band-edge matrix elements determine the low-frequency dielectric constant, the discrepancy in the peaks is, therefore, largely the result of our linear interpolation approximation. The problem with this approximation is that al-

though it provides a good average energy dispersion relation, it sometimes produces a poor value for the density of states. This discrepancy also accounts for the difference in the shapes of the two curves. Nevertheless, despite the approximations involving the matrix elements and energy dispersion relations, the results of the two models are comparable for GaAs, InAs, and InP and assert the validity of our model.

B. The zero-frequency dielectric constant: $\epsilon_1(0)$

In Table II we give $\epsilon_1(0)$ at 5 K for the five III-V compounds. We also list the experimental values and the individual contributions of the three regions. Only the GaAs experimental data are 5 K values; for the other four materials the values are extrapolated from 300 K using the GaAs $\epsilon_1(0)$ temperature dependence. The theoretical values are uniformly low with an average error of $\sim 7.5\%$. The error is partly due to the omission of all high-energy transitions. The errors for AlAs, InP, and GaP are small because of the overestimation of the virtual transitions corresponding to the E_2 peak. This effect is particularly pronounced for GaP where the E_2 transitions compensate for the small contribution from the E_1 transitions. For GaAs, the error results also from its weak E_1 contribution. For InAs the error is $\sim 12\%$ in spite of its large E_1 peak. This probably stems from the fact that its E_2 peak is small and $\epsilon_1(0)$ of this small gap material is affected most by the neglect of higher-band contributions in our model.

The valley contributions are split up according to the partition of the Brillouin zone as presented in Sec. III. For all materials, the L region contributes approximately 60–70% to the total value of the dielectric constant while the Γ region accounts for about 5–10%. This general trend is also confirmed for optical frequencies corresponding to the Γ energy gap. Thus, the index of refraction is essentially determined by the band structure away from the center of the Brillouin zone. The implications of these results are important for complex materials and structures, such as ternaries, quaternaries, and superstructures, where the modifications of the electronic structure at L and X , rather than at Γ , produce the variations in the index of refraction. An additional consequence of these results is a better understanding of the validity of the Penn model.³⁶ The latter is based on a three-dimensional (3D), nearly-free-electron, band model. The Brillouin zone is approximated as a sphere and the band edges are dis-

TABLE II. Theoretical and experimental $\epsilon_1(0)$ values at 5 K for five III-V compounds. Also included are the calculated individual contributions of the Γ , X , and L regions to $\epsilon_1(0)$ for each of the five compounds.

Material	$\epsilon_1(0)$ (theory)	$\epsilon_1(0)$ (expt.)	% error	Contributions of the three regions		
				L	X	Γ
GaAs	8.68	10.60	18.1	6.01	1.25	0.41
AlAs	7.42	7.90	6.1	5.12	1.16	0.14
InP	9.13	9.27	1.5	6.68	1.12	0.33
InAs	10.10	11.49	12.1	7.26	0.94	0.91
GaP	8.77	8.80	0.4	6.30	1.21	0.25

placed from the center to the surface of the zone, resulting in a singular density of states around the band gap. It is pointed out³⁶ that such a singular behavior in a 3D system would not appear if the gap is placed at the center of the zone. It is the fortuitous coincidence of this singular density of states at the edge of the zone with the actual description of the states around the L and K points, characterized by large interband matrix elements and densities of states, which provides the Penn model with its validity and success in calculating the dielectric constant.

V. CONCLUSION

We have developed a general model of the dielectric constant of III-V compounds, using a hybrid method which combines the $\mathbf{k}\cdot\mathbf{p}$ method with a nonlocal pseudopotential calculation. We have introduced a technique which partitions the Brillouin zone into three regions by expanding the energy bands and matrix elements about the Γ , X , and L symmetry points. In order to keep the expressions simple and limited to small basis sets, expansions about the K and W points are also performed and included in the X and L regions. The real and imaginary parts of the dielectric constant are calculated by determining the individual contributions of each region to the dielectric constant. The partition method enables us to determine easily the dependence of the dielectric constant on the form of the band structure. The advantage of this

method is its flexibility, enabling it to analyze more complex structures and materials, such as heterostructures and alloys.

Our results for the imaginary part of the dielectric constant are consistent with other one-electron band-structure techniques. The peak at E_1 is broader and weaker than the experimental peak and is mainly influenced by the transverse-band curvature at the L point. The E_2 peak is slightly stronger and shifted with respect to the experimental peak, being mostly determined by the density of states around the special point $(\frac{3}{4}, \frac{1}{4}, \frac{1}{4})$. The real part of the dielectric constant at low frequency is strongly influenced by the band structure at the edges of the Brillouin zone, with a contribution of 90–95% for the X and L regions and only 5–10% for the Γ region. Consequently, except for optical absorption in the vicinity of the Γ gap, most of the optical properties of materials, especially the index of refraction, are essentially determined by the electronic structure around the L point, rather than at the center of the Brillouin zone.

ACKNOWLEDGMENTS

The authors are indebted to K. Hess and N. Holonyak, Jr. for encouragement and fruitful discussions. The support of the National Aeronautics and Space Administration is gratefully appreciated.

- ¹H. R. Philipp and H. Ehrenreich, *Phys. Rev.* **129**, 1550 (1963).
- ²B. O. Seraphin and H. E. Bennett, in *Semiconductors and Semimetals*, Vol. 3, edited by R. K. Willardson and A. C. Beer (Academic, New York, 1967), p. 499.
- ³B. Monemar, *Solid State Commun.* **8**, 1295 (1970).
- ⁴R. E. Fern and A. Onton, *J. Appl. Phys.* **42**, 3499 (1971).
- ⁵H. C. Casey, Jr. and M. B. Panish, *Heterostructure Lasers, Part B* (Academic, Orlando, 1978).
- ⁶D. J. Stukel and R. N. Euwema, *Phys. Rev.* **186**, 754 (1969); **188**, 1193 (1969).
- ⁷T. C. Collins, D. J. Stukel, and R. N. Euwema, *Phys. Rev. B* **1**, 724 (1970).
- ⁸Y. F. Tsay, A. J. Corey, and S. S. Mitra, *Phys. Rev. B* **12**, 1354 (1975).
- ⁹J. R. Chelikowsky and M. L. Cohen, *Phys. Rev. B* **14**, 556 (1976).
- ¹⁰C. S. Wang and B. M. Klein, *Phys. Rev. B* **24**, 3417 (1981).
- ¹¹L. Esaki and R. Tsu, *IBM J. Res. Dev.* **14**, 61 (1970).
- ¹²L. Esaki and L. L. Chang, *Crit. Rev. Solid State Sci.* **6**, 195 (1976).
- ¹³N. Holonyak, Jr., W. D. Laidig, M. D. Camras, J. J. Coleman, and P. D. Dapkus, *Appl. Phys. Lett.* **39**, 102 (1981).
- ¹⁴K. B. Kahen, J. P. Leburton, and K. Hess, *Superlatt. Microstruct.* **1**, 289 (1985).
- ¹⁵E. O. Kane, *J. Phys. Chem. Solids* **1**, 82 (1956).
- ¹⁶E. O. Kane, in *Semiconductors and Semimetals*, Vol. 1, edited by R. K. Willardson and A. C. Beer (Academic, New York, 1966), p. 71.
- ¹⁷G. Dresselhaus, *Phys. Rev.* **100**, 586 (1955).
- ¹⁸P. O. Löwdin, *J. Chem. Phys.* **19**, 1396 (1951).
- ¹⁹D. J. Chadi, *Solid State Commun.* **20**, 361 (1976).
- ²⁰D. J. Chadi, *Phys. Rev. B* **16**, 3572 (1977).
- ²¹G. Dresselhaus, A. F. Kip, and C. Kittel, *Phys. Rev.* **98**, 368 (1955).
- ²²J. S. Blakemore, *J. Appl. Phys.* **53** R123 (1982).
- ²³E. D. Pallik and R. F. Wallis, *Phys. Rev.* **123**, 131 (1961).
- ²⁴C. W. Litton, R. B. Denis, and S. D. Smith, *J. Phys. C* **2**, 2146 (1969).
- ²⁵C. R. Pidgeon, D. L. Mitchell, and R. N. Brown, *Phys. Rev.* **154**, 737 (1967).
- ²⁶J. Leotin, R. Barbaste, S. Askenazy, M. S. Skolnick, R. A. Stradling, and J. Tuchendler, *Solid State Commun.* **15**, 693 (1974).
- ²⁷A. Onton, *Phys. Rev.* **186**, 786 (1969).
- ²⁸F. Bassani and G. P. Parravicini, *Electronic States and Optical Transitions in Solids* (Pergamon, Oxford, 1975), Chap. 5.
- ²⁹D. E. Aspnes and A. A. Studna, *Phys. Rev. B* **27**, 985 (1983).
- ³⁰B. Velicky and J. Sak, *Phys. Status Solidi* **16**, 147 (1966).
- ³¹W. Hanke and L. J. Sham, *Phys. Rev. B* **21**, 4656 (1980).
- ³²K. B. Kahen and J. P. Leburton (unpublished).
- ³³D. E. Aspnes, *Phys. Rev. Lett.* **31**, 230 (1973).
- ³⁴J. R. Chelikowsky and M. L. Cohen, *Phys. Rev. Lett.* **31**, 1582 (1973).
- ³⁵C. Hermann and C. Weisbuch, *Phys. Rev. B* **15**, 823 (1977).
- ³⁶D. R. Penn, *Phys. Rev.* **128**, 2093 (1962).